

Trapped Exciton and Large Birefringence in Cl₂-NDI Revealed by Optical Spectroscopy

Marko Pinterić,¹ Seulki Roh,^{*1} Ece Uykur, Nis Hauke Hansen, Jens Pflaum, Matthias Stolte, Frank Würthner, and Martin Dressel

Cite This: *J. Phys. Chem. C* 2020, 124, 17829–17835

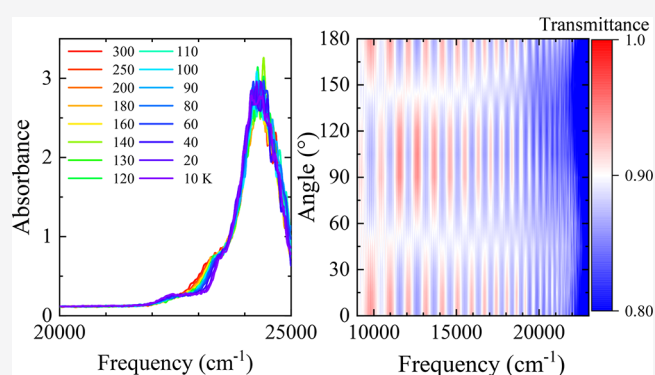
Read Online

ACCESS |

Metrics & More

Article Recommendations

ABSTRACT: The n-type organic semiconductor, β -phase single crystalline dichloro naphthalene diimide, Cl₂-NDI, is investigated in a broad frequency range via optical spectroscopy. The temperature-dependent absorbance spectra reveal the appearance of new molecular vibration modes; several of them exhibit a pronounced splitting and abnormal red shift. In the visible spectral range, we observe a splitting of the *J*-band upon cooling, which we attributed to self-trapped excitons via coupling between free excitons and molecular vibrations or trapping by disorder induced Lévy states. Additionally, we discover a strong birefringence of these crystals by pronounced polarization beat over a wide frequency range.



INTRODUCTION

Aggregated organic materials provide rich optoelectronic phenomena such as pleochroism, superradiance, and photovoltaic effects that can be used in a large variety of various optical as well as optoelectronic applications.^{1–5} Consequently, numerous studies have been conducted in this regard. In aggregated molecular systems the structure composed of π -stacked conjugated molecules significantly influences the material properties, including the electronic and the optical response. Thus, it is important to investigate the relation between the structure and the electronic properties in order to reach an understanding of the interrelating mechanisms for further utilizations of these systems.

This close relation between structure and optoelectronic properties of π -conjugated organics has been successfully explained by the molecular exciton model.^{4–8} Due to the dipolar-coupling between molecules, the energy of the excited monomer state splits into two levels, one of higher and one of lower energy compared to the monomer energy level. Depending on their stacking pattern, the aggregations can be divided into two types, *J*- and *H*-aggregates; the classification is based on the slipping angle, Θ , between two adjacent molecules. In the case of π -stacking, one obtains *J*-aggregates for $\Theta < 54.7^\circ$ and *H*-aggregates for $\Theta > 54.7^\circ$, as depicted in Figure 1a. In *H*-aggregates, the molecules are arranged in a face-to-face manner. In *H*-aggregates, optical excitations to the lower energy level are forbidden; thus, only transitions to the higher energy state can be observed. This results in a hypsochromic shift (blue shift), denoted as the *H*-band in

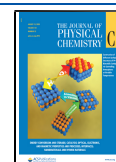
the absorption spectra. Conversely, if the molecules are aligned in a head-to-tail way, the splitting of the monomer energy occurs in a similar way; however, in this case only excitations to the lower energy band are allowed, leading to a bathochromic shift (red shift), the so-called *J*-band (Figure 1b).

In this sense, a prototypical n-type organic semiconductor, *N,N'*-bis(heptafluorobutyl)-2,6-dichloro-1,4,5,8-naphthalene tetracarboxylic diimide (abbreviated Cl₂-NDI) (Figure 1c) serves as a good platform to study the interrelation between packing and the resulting optical characteristics since it crystallizes in two different structural phases, α and β , depending on its stacking fashion, and its electronic properties vary greatly with the corresponding π -stacking.^{9–11} The α -phase belongs to a monoclinic space group $P2_1/c$ and has a herringbone stacking motif, where the angle between the NDI skeleton and the fluoroalkyl chain is 129.7° . In this herringbone packing, the π - π stacking distance is 3.27 \AA with a slipping angle of 62° with two molecules in a unit cell (Figure 1e,g). The oblique alignments in the herringbone packing yield both *J*- and *H*-bands in the optical spectra, i.e., the Davydov splitting¹² as illustrated in Figure 1b. [The *J*-band

Received: June 7, 2020

Revised: July 13, 2020

Published: July 20, 2020



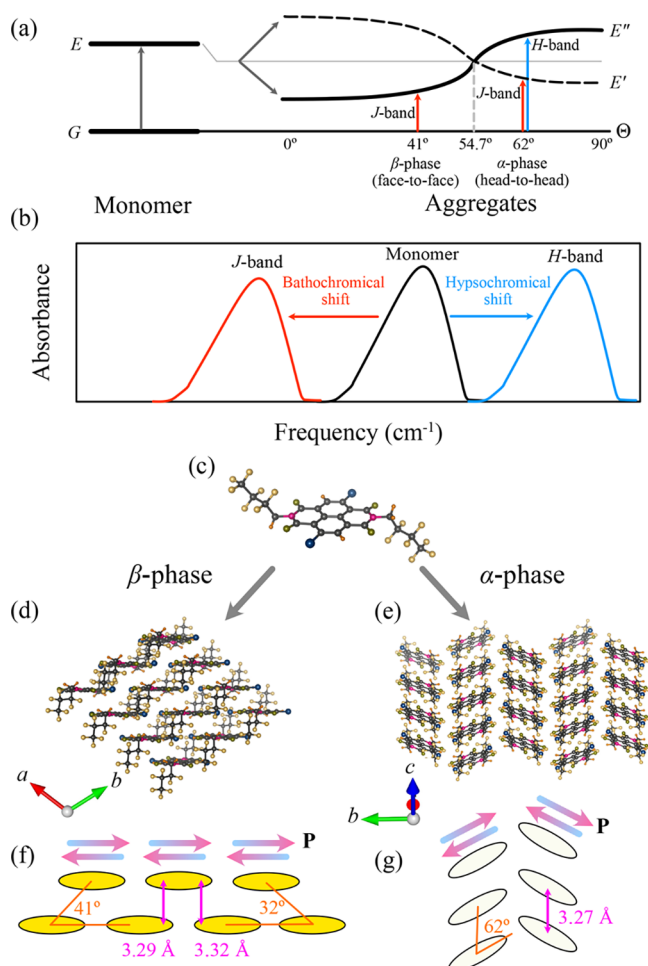


Figure 1. Crystal structure of Cl₂-NDI (dichloro naphthalene diimide) and optical excitations in aggregates. (a) Electronic levels for *J*- and *H*-aggregates and corresponding optical excitations for the α - and β -phases. For the α -phase, both excitations to E' and E'' are allowed, due to the oblique stacking. (b) Absorbance spectra for *J*- and *H*-bands with respect to the monomer band. (c) Structure of a single Cl₂-NDI molecule. The gray, magenta, blue, yellow, and orange atoms represent C, N, Cl, F, and H, respectively. Parts d and f, and parts e and g, show aggregated structures of Cl₂-NDI in the β - and α -phases, respectively. The directions of molecular dipole moments are depicted in color gradient arrows.

and *H*-band in *H*(-*J*)-aggregate is also called as lower and higher *H*(-*J*)-band, in the case of their coexistence.] On the other hand, the β -phase is a triclinic system with $P\bar{1}$ space group. The torsion angle between the NDI skeleton and the fluoroalkyl chain increases to 133.9°, leaving one molecule in a unit cell. This phase yields a two-dimensional brick wall packing with slipping angles of 41° and 32° and π - π stacking distances of 3.29 and 3.32 Å, respectively (Figure 1d,f). Slipping angles of less than 54.7° in the β -phase favor *J*-coupling; hence, only absorption and emissions by the lower band (*J*-band) of the *J*-aggregate are pronounced. The transition from α - to β -arrangement was realized by heating up the sample above 170 °C. In the opposite direction, the transition from β - to α -phase can also be achieved by cooling down the sample to liquid nitrogen temperature. However, the thermally induced phase transition back to α -phase appears to be hindered and, thus, takes very long time (several months).⁹ Previous studies reported high electron mobilities at ambient

conditions up to 8.6 and 3.5 cm² V⁻¹ s⁻¹ in the α - and β -phase, respectively, where the significant variation between these values is an indication for the different electronic structure of the two polymorphs.^{9,11}

Here, we report the optical properties of single crystalline β -phase Cl₂-NDI via optical transmittance experiments in a wide frequency range from the far-infrared to visible. Optical spectroscopy is sensitive to both the molecular vibration and the electronic state; thus, one can access the interrelation between the electronic and vibrational excitations and its dependence of the crystalline packing. Upon cooling, we observed splittings and anomalous red shifts in the molecular vibrational modes at low frequencies and a splitting of the excitonic *J*-band at high frequencies. These two observations together imply that excitons are localized via coupling with the intermolecular vibrations, i.e., phonon modes, or disorder driven Lévy state. Additionally, polarization-dependent transmittance spectra exhibit polarization beats, manifesting a large birefringence over a wide spectral range. Our results provide insight into the correlation between the lattice vibration and the excitonic state in the aggregated organics; furthermore, we unveil the unique optoelectronic properties in this system.

METHODS

Single crystalline Cl₂-NDI samples in the β -phase are prepared from purified Cl₂-NDI by physical vapor transport method at 235 °C in ambient atmosphere.^{9,13} For the optical measurements, a Bruker Vertex 80v FTIR spectrometer attached to a Hyperion microscope was employed to record the transmittance of a thin (~15 μm) single crystal of Cl₂-NDI in a wide frequency range from 100 to 25 000 cm⁻¹. The temperature was controlled by an Oxford Microstat, and the optical measurements were performed at a typical cooling rate of 1 K min⁻¹. The lowest temperature of approximately 10 K was reached about 10 h after the start of the cooling cycle. Suitable linear polarizers were used for the polarization-dependent measurements. The absorbance, $\alpha(\omega)d$, was calculated by using the Beer-Lambert law, $\alpha(\omega)d = -\ln(T)$, where α is the absorption coefficient, d is the thickness of the sample, and T is the measured transmittance normalized to the vacuum transmittance,¹⁴⁻¹⁷ as the reflectivity of the sample is negligibly small.

RESULTS AND DISCUSSION

Before we focus on electronic excitations in the visible range of the spectrum, let us briefly present the vibrational features in the infrared region and discuss the implications for the structure.

Vibrational Modes and Structural Instability. The temperature evolution of the infrared-active vibrational modes located at low frequencies is displayed in Figure 2a. Due to a large number of atoms in a unit cell, numerous modes are present in the optical spectra. With decreasing temperature, most of the features exhibit a sharpening and blue shift by a reduced lattice anharmonicity. However, some irregular temperature dependence was observed in several modes. For closer inspection, we plotted representative modes in larger scales in Figure 2b-d. In Figure 2b, three modes are marked by vertical dashed gray lines and labeled by A, B, and C. The A-mode develops as a shoulder below $T = 160$ K and eventually splits as an individual mode; the original resonance remains at the same frequency. Meanwhile, two features (B

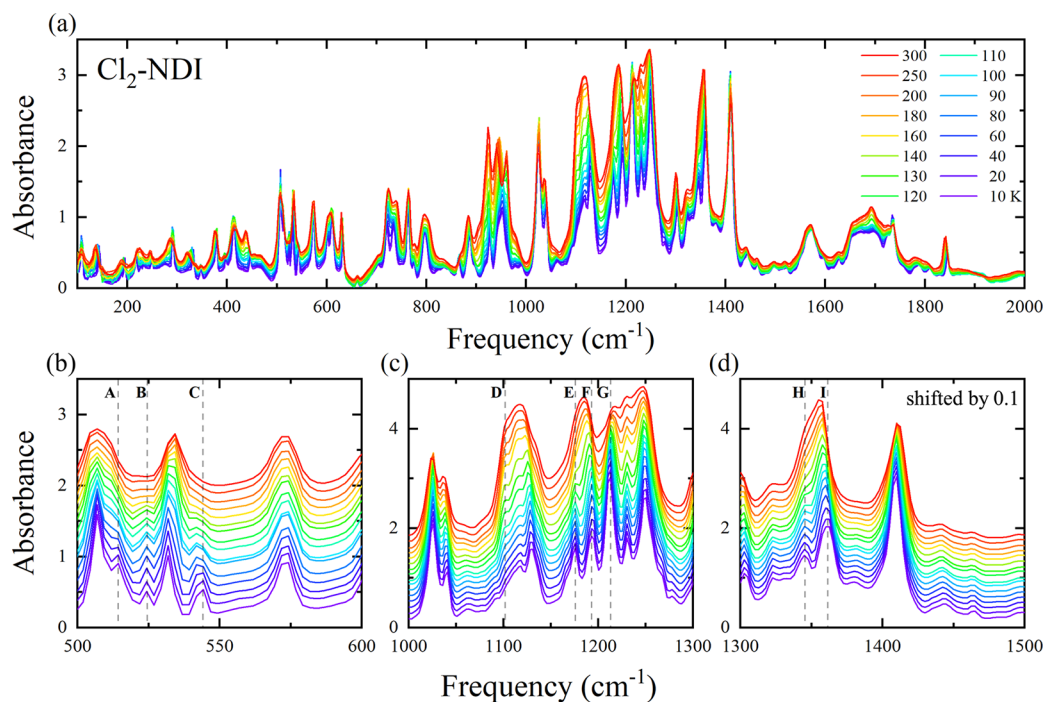


Figure 2. (a) Overview of the absorbance spectra of vibrational modes in $\text{Cl}_2\text{-NDI}$ in the fingerprint range for various temperatures as indicated. (b–d) Magnified views of particular vibrational features. The selected modes are labeled from A to I and marked with vertical dashed gray lines. The curves are vertically shifted for clarity.

and C) appear below 160 K, as well. In Figure 2c we observe that D disappears by losing the spectral weight on lowering the temperature, while E and F split into two individual modes. The G feature shows an anomalous red shift upon cooling, which implies a structural instability in this system. Also the modes H and I in Figure 2d split into two individual oscillations where both lose their spectral weight considerably.

In the quasiharmonic model of lattice vibrations, the oscillation frequency, ω_c , depends on the temperature due to thermally induced changes in volume, V . The relation between the variation in volume and vibrational frequency of the mode can be written as $\Delta\omega_c/\omega_c = -\gamma\Delta V/V$, where γ is the Grüneisen parameter. Usually γ is positive, yielding a blue shift of ω_c upon cooling. Hence, the unusual red shift observed for the G-mode can be interpreted as a strong anharmonicity near a structural instability similar to reports in other systems.^{17–20} Along with the pronounced red shift, the splitting of the molecular vibrational modes is a direct consequence of a reduced lattice symmetry, i.e., a structural transition.

Electronic Properties. In the visible energy range above 20 000 cm^{-1} , pronounced electronic excitations are observed in the absorption spectrum as displayed in Figure 3a. The main band at 24 400 cm^{-1} changes only slightly when the temperature is reduced; it can be explained within the framework of the aggregate model and the optical excitations of π -conjugated supramolecular assemblies.^{4–8} Surprisingly, additional features are identified around 23 000 cm^{-1} , which we assign to strong excitonic absorption. They deserve a thorough analysis and interpretation, because they are composed of electronic and vibronic orders and play an important role on the optical properties of these molecular aggregates.

Molecular Interaction. For years, π -conjugated organic molecules and their aggregates have attracted great attention,

and the optical properties of these aggregates have been investigated in detail for many configurations. It has been realized that the intermolecular interactions and the molecular packing arrangement (in the current case, within the crystal unit cell) are strongly interdependent and that both steer collective excitations, such as excitons, and their dynamics in the molecular solid state.

Once two identical molecules come in close proximity to each other, the transition dipolar moments of these molecules start to interact with each other creating an excitonic coupling. The relative orientation of these molecules causes the splitting of the energy levels of the individual molecules, as demonstrated in Figure 1a.

In the case of a face-to-face alignment (H -aggregate) the parallel dipoles repel each other and form a state of higher energy, which is characterized by a strong dipole moment, i.e., strong absorption. In contrast, the antiparallel dipoles of an H -type aggregate attract each other, which lowers the energy of the resulting state and cancels its transition dipole leading to a weaker absorption. This results in a net blue shift of the energy levels of the uncoupled monomers. The other possible arrangement is the head-to-tail arrangement that creates an opposite effect causing a net red shift relative to the energy level of the isolated monomers. Molecular aggregates causing a red shift of the bands are commonly referred to as the J -aggregate, whereas aggregates leading to a blue shift of the bands are the H -aggregates. The relative energy bands of these different aggregates with respect to their uncoupled monomer arrangement are shown in Figure 1b. For the intermediate orientations, termed oblique—such as in case of the herringbone packing of the α -phase in $\text{Cl}_2\text{-NDI}$ —the energy shift depends on both the intermolecular distance and the angles between the dipoles. Such excitonic coupling between more than two molecules allows the absorbance spectrum to contain a mixture of J - and H -type optical properties (see

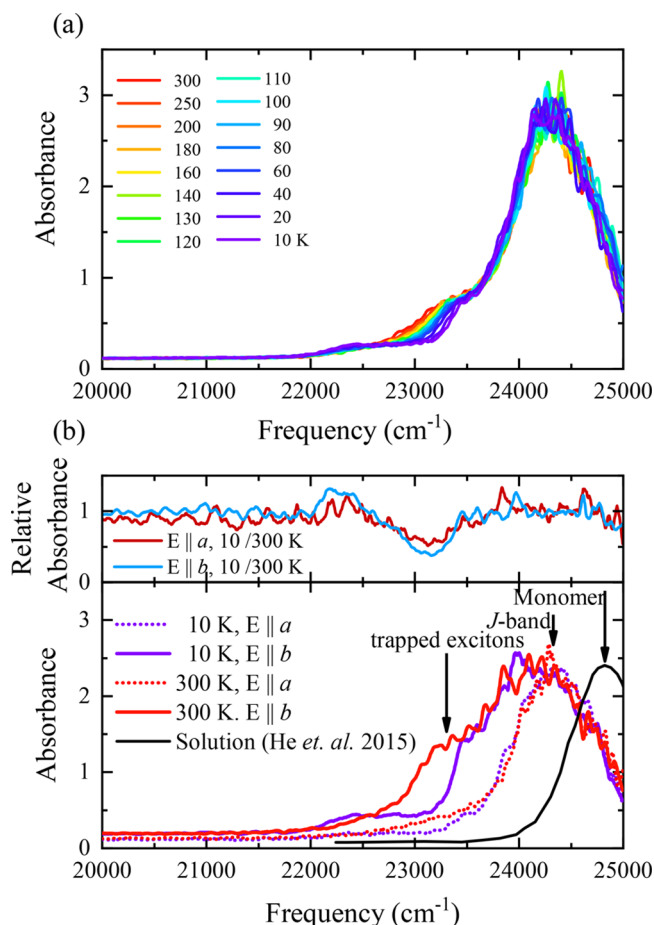


Figure 3. Exciton absorption in Cl₂-NDI. (a) Temperature-dependent evolution of excitons measured without a polarizer. Absorbance spectra measured by polarized light along the *a*- and *b*-axes are plotted in lower panel of part b for selected temperatures. The black line represents the monomer absorption taken from ref 9. The upper panel displays the relative absorbance at 10 K versus 300 K for both *a*- and *b*-axes.

Figure 1a). In this case, in optical spectra along distinct directions commonly either the signature of the *H*- or of the *J*-aggregate is observed, the Davydov components.¹²

The orientation is accounted for by a simple dipole model, where intermolecular interaction strength is given by $\kappa^2 = (1 - 3 \cos^2 \Theta)^2$. For the “magic angle” of 54.7°, the dipoles appear to be noninteracting. As demonstrated in Figure 1a, for smaller angles the absorption bands dominating the spectra are associated with the *J*-coupling, while for larger angles bands are favorable that are associated with the *H*-coupling.^{5,21–24}

Absorption Edge. If we now turn to the present example of Cl₂-NDI, we see from Figure 3 that the strongest absorption mode appears around 24 400 cm⁻¹. It can be associated with the *J*-aggregate, as it shows a red shift (~ 500 cm⁻¹, ~ 60 meV) with respect to the monomer in solution (depicted by the black solid curve in the lower panel of Figure 3b). Considering the slip angle of the molecules arranged within the β - and α -phases, we attributed this strong absorption feature to the β -phase of Cl₂-NDI, as it satisfies the necessary condition of slip angle, that is, $\Theta < 54.7^\circ$.^{6,9,11}

Having assigned the *J*-band, we can focus on two smaller modes located below the *J*-band. One is the shoulderlike peak located at 23 400 cm⁻¹, whose intensity is suppressed with

cooling down. The other one can be found at 22 400 cm⁻¹; it appears at low temperatures only. In the lower panel of Figure 3b, polarization-dependent spectra measured along the *a*- and *b*-axes at *T* = 10 and 300 K are displayed. The two modes observed are more pronounced along the *b*-direction; nevertheless, if we normalize the absorbance by the absorbance spectra measured at 300 K, one can see that both polarizations show the same trend. In fact, this shoulder splits into two separate modes rendering a steplike feature at low temperatures. The origin of this shoulder-peak and its split evades a complete understanding at this point. We suggest that it signals trapped exciton states. In particular, either exciton–phonon coupling induced exciton polarons or disorder driven Lévy states which have been reported previously.^{5,7,24–30}

Exciton Polarons. In aggregates, excitons are delocalized; thus, several molecules are linked forming a coherent excitonic state (*J*-band in this situation). If we now consider the exciton–phonon coupling—in our case, to the intermolecular vibrations—excitons can become localized. This localization causes the atomic displacement in the vicinity of the localized exciton to decrease the potential.^{7,31,32} Simultaneously, the reduced potential tends to localize the exciton even further; in other words the exciton and phonon couple to each other forming a trapped state, i.e., a polaron. If the coupling between exciton and phonon is strong enough, the exciton can be trapped due to the potential deformed by itself, creating a self-trapped state.^{7,27,32,33}

Polarons have been observed previously in other materials, and depending on the radius of the polarons they are divided into large and small polarons.^{34–38} The self-trapped case corresponds to the small polaron, with a radius of about a few nm and with a characteristic energy scale of a few eV, i.e., significantly larger than the corresponding transfer integral. The self-trapped exciton state has lower energy than a delocalized exciton since the deformed lattice favors the localized state. Due to this coupling between the phonon and exciton, the self-trapped state is located in a different position of momentum space than the ground state. Therefore, optical transitions require assistance from the phonon absorption to be detected in the absorption measurement (Franck–Condon principle). For this reason, the detected signal usually is small compared to the original absorption signal. The lattice distortion features a shift or a splitting in the phonon spectra, as was observed in our vibrational spectra (cf. Figure 2). In particular, the separation of the self-trapped mode is about 900 cm⁻¹, which implies that the coupled phonon has a resonance frequency at 900 cm⁻¹. Indeed, the molecular vibrations at 950 cm⁻¹ exhibit abrupt changes with decreasing temperature suggesting their relation to the exciton modes. Note, this self-trapping process differs from the previously reported crystal edge trapping³⁹ since the temperature-dependent splitting in our spectra is not expected from the geometrical effect; furthermore, the localization occurs along both crystallographic directions regardless of the edge direction.

Lévy States. Another plausible explanation could come from the small changes in molecular structure, which result in a lower *J*-band. In this case, the alteration in the structure leads to a modified stacking of the molecules. However, most of the spectral weight remains in the *J*-band, implying that only a small portion of the molecules actually undergoes this transition resulting in a mixed phase. This structural variation gives disorder to the system by fluctuating the intermolecular interaction (off-diagonal disorder). Such a disorder could

broaden the distribution of exciton bands, by introducing a heavy-tailed Lévy distribution.^{5,24,28–30} The Lévy distribution in *J*-aggregates results in a single outlier state which is much lower energy state than other exciton states, i.e., a Lévy state.^{5,28} This state can be considered as a trapped exciton state caused by the large energy difference between the Lévy state and rest of the states in exciton bands. Different length scales of the multiple structural domains in the mixed phase will possibly form multiple Lévy states with slightly different energies rendering peaklike features in the absorption spectra. Therefore, in this scenario, the observed two smaller modes could be interpreted as optical excitations to the Lévy states. The structural transition observed in our molecular vibration spectra also supports this idea.

The structural transition could possibly be α -phase transition or a local precursor of it. However, a complete transition to the α -phase is excluded because no *H*-band appears in our spectra, which should be located near the monomer band.^{9,11} In addition, two molecules in a unit cell in the α -phase should show anisotropic lower and higher *H*-bands (Davydov components) whereas in our case it is nearly isotropic. Still, we do not exclude the possibility of a phase transition to the α -phase on local length scales. In this case, the two smaller modes could be related to the vibronic side bands of *H*-band expected in the multimolecule Frenkel polaron picture.^{4,5} In this picture, strong coupling between the vibrational mode and exciton renders a small first absorption band at lower energies, while most of the spectral weight moves to the higher energy bands in the *H*-aggregate. However, the local limit of the phase transition to the α -phase should restrict this effect to be small. Our study of Cl₂-NDI suggests two scenarios which are exciton polarons and Lévy states of excitons. Clarification of these phenomena still remains to be fulfilled in combination with other experimental techniques. Regardless, our observations reveal the close relation between the structure and excitonic transition in this system.

Birefringence. Our transmission data reveal another interesting optical phenomenon: β -phase single crystalline Cl₂-NDI exhibits a pronounced birefringence over a wide frequency range. Figure 4a displays the polarization-dependent transmittance as a function of frequency measured under ambient conditions. The polarization beat is well pronounced over the entire spectra due to a phase shift by the birefringent material.^{40–43} Calculating the index of refraction for 0° and 90° at 11 000 cm⁻¹—assuming no extinction, for simplicity—yields $n_1 = 1.58$ and $n_2 = 2.22$, respectively. The birefringence $\Delta n = 0.64$ is very large considering that the birefringences of usual optical materials are around 0.1–0.3,^{44–46} where some organic aggregates show values comparable to our Cl₂-NDI.^{43,47} Note that this oscillation is distinct from the outcome of a Fabry–Pérot etalon, which accounts for the internal multireflection of the sample. As a matter of fact, Fabry–Pérot oscillations are also observed as magnified in the inset of Figure 4a. They exhibit a small frequency interval of 150 cm⁻¹, which relates to the sample thickness, *d*, via the simple relation $\Delta\nu = 1/2nd$ in the normal incidence. Using $n = 1.9$ (average of the n_1 and n_2) we obtain $d = 16 \mu\text{m}$ in good agreement with the thickness of our crystal measured by a microscope (15 μm). For a better illustration, Figure 4b displays a color map of the transmittance as a function of frequency and polarization angle. Two different optical axes can be identified by the two horizontal patterns generated at

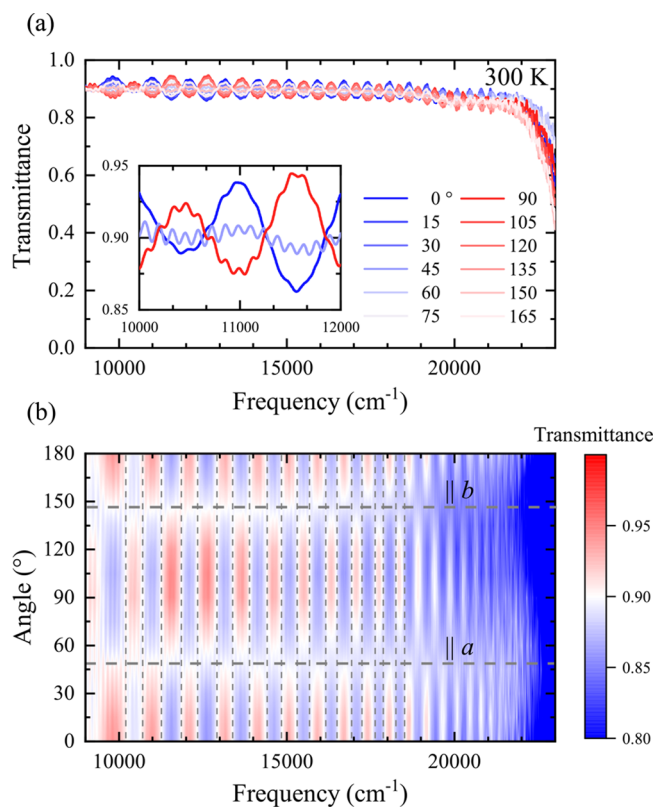


Figure 4. (a) Polarization-dependent transmittance spectra at 300 K. The inset displays a magnified view for 0°, 45°, and 90°. (b) Color plot of the transmittance as a function of frequency and rotational angle. Horizontal dashed gray lines denote the *a*- and *b*-axes. Vertical dashed gray lines represent the frequencies, where the nodes of the polarization beat are located.

45° and 135°, which correspond to the crystal axes *a* and *b*, respectively. At these two angles, the spectra show smooth curves without beating, implying that the net phase shift vanishes along these directions. The beat intensity is most strongly pronounced for the orientations 0° and 90° with opposite phases. This inference diminishes as the frequency rises and reaches the excitonic absorption; eventually it is completely screened. The nodes appearing in the transmittance spectra as vertical dashed gray lines are those frequencies at which the incident light turns into circularly polarized light, as the net phase shift becomes $\pm\pi/4$.⁴¹ In other words, our Cl₂-NDI crystal turns the linearly polarized light into a circularly polarized light at multiple frequency points.

The birefringent material can be utilized as waveplates, which delays the phase for the slow-axis compared to that of fast-axis. The combination of the quarter-waveplate and the linear polarizer can turn the light into circularly polarized light. The common problem of birefringence is the narrow working frequency. Usually, one needs to match the birefringence $\Delta n = n_2 - n_1$ and the thickness, in order to obtain the phase shift $2\pi\Delta nd/\lambda = m$ where m is the integer. Since the phase shift also is subject to the wavelength, making a broadband waveplate is challenging. However, our Cl₂-NDI sample exhibits multiple nodes where the light becomes circularly polarized over a broadband frequency range, from mid-infrared to visible frequencies, with nearly 90% of transmittance, promoting this system as a prime platform for broadband waveplate applications.

CONCLUSIONS

Comprehensive optical investigations on β -phase Cl₂-NDI single crystals have been performed by temperature- and polarization-dependent infrared spectroscopy. A splitting and red shift of several infrared active vibrational modes are detected upon cooling, as well as the splitting of the J-band in two individual modes at low temperatures. We suggest two possible interpretations: (i) A coupling between intermolecular vibrational modes and excitonic features forms self-trapped excitons appearing in Cl₂-NDI at low temperatures. (ii) Low-temperature structural disorder introduces a heavy-tailed Lévy distribution in excitonic bands resulting in Lévy states. Our findings demonstrate a close relation between structure and electronic properties. In addition, polarization-dependent transmittance experiments reveal a large birefringence extending over a wide frequency range; this makes Cl₂-NDI interesting for applications in various optical devices.

AUTHOR INFORMATION

Corresponding Author

Seulki Roh – 1. Physikalisches Institut, Universität Stuttgart, 70569 Stuttgart, Germany; orcid.org/0000-0003-0424-614X; Email: seulki.roh@pi1.uni-stuttgart.de

Authors

Marko Pinterić – 1. Physikalisches Institut, Universität Stuttgart, 70569 Stuttgart, Germany; Faculty of Civil Engineering, Transportation Engineering and Architecture, University of Maribor, SI-2000 Maribor, Slovenia

Ece Uykur – 1. Physikalisches Institut, Universität Stuttgart, 70569 Stuttgart, Germany

Nis Hauke Hansen – Experimentelle Physik VI, Universität Würzburg, 97074 Würzburg, Germany

Jens Pflaum – Experimentelle Physik VI, Universität Würzburg, 97074 Würzburg, Germany

Matthias Stolte – Institut für Organische Chemie and Center for Nanosystems Chemistry, Universität Würzburg, 97074 Würzburg, Germany

Frank Würthner – Institut für Organische Chemie and Center for Nanosystems Chemistry, Universität Würzburg, 97074 Würzburg, Germany; orcid.org/0000-0001-7245-0471

Martin Dressel – 1. Physikalisches Institut, Universität Stuttgart, 70569 Stuttgart, Germany

Complete contact information is available at: <https://pubs.acs.org/10.1021/acs.jpcc.0c05165>

Author Contributions

[†]M.P. and S.R. contributed equally.

Notes

The authors declare no competing financial interest.

ACKNOWLEDGMENTS

We thank G. Untereiner for technical support and T. Biesner for fruitful discussions. The work was supported by the Deutsche Forschungsgemeinschaft (DFG) via DR228/48-1 (Stuttgart) and PF385/11-1 (Würzburg). E.U. acknowledges the European Social Fund and the Baden-Württemberg Stiftung for the financial support of this research project by the Eliteprogramme. J.P. and F.W. acknowledge the Bavarian State Ministry for Science and the Arts for funding within the collaborative research network “Solar Technologies go Hybrid” (SolTech).

REFERENCES

- (1) Fratini, S.; Nikolka, M.; Salleo, A.; Schweicher, G.; Sirringhaus, H. Charge transport in high-mobility conjugated polymers and molecular semiconductors. *Nat. Mater.* **2020**, *19*, 491–502.
- (2) Doria, S.; Sinclair, T. S.; Klein, N. D.; Bennett, D. I.; Chuang, C.; Freyria, F. S.; Steiner, C. P.; Foggi, P.; Nelson, K. A.; Cao, J.; et al. Photochemical Control of Exciton Superradiance in Light-Harvesting Nanotubes. *ACS Nano* **2018**, *12*, 4556–4564.
- (3) Cannon, B. L.; Patten, L. K.; Kellis, D. L.; Davis, P. H.; Lee, J.; Graugnard, E.; Yurke, B.; Knowlton, W. B. Large Davydov Splitting and Strong Fluorescence Suppression: An Investigation of Exciton Delocalization in DNA-Templated Holliday Junction Dye Aggregates. *J. Phys. Chem. A* **2018**, *122*, 2086–2095.
- (4) Hestand, N. J.; Spano, F. C. Expanded Theory of H- and J-Molecular Aggregates: The Effects of Vibronic Coupling and Intermolecular Charge Transfer. *Chem. Rev.* **2018**, *118*, 7069–7163.
- (5) Brixner, T.; Hildner, R.; Köhler, J.; Lambert, C.; Würthner, F. Exciton Transport in Molecular Aggregates – From Natural Antennas to Synthetic Chromophore Systems. *Adv. Energy Mater.* **2017**, *7*, 1700236.
- (6) Kasha, M.; Rawls, H. R.; Ashraf El-Bayoumi, M. The exciton model in molecular spectroscopy. *Pure Appl. Chem.* **1965**, *11*, 371–392.
- (7) Malyukin, Y. V.; Sorokin, A. V.; Semynozhenko, V. P. Features of exciton dynamics in molecular nanoclusters (J-aggregates): Exciton self-trapping (Review Article). *Low Temp. Phys.* **2016**, *42*, 429–440.
- (8) Sorokin, A. V.; Yefimova, S. L.; Malyukin, Y. V. *Encyclopedia of Polymer Science and Technology*; John Wiley & Sons, Inc.: Hoboken, NJ, 2018; pp 1–33.
- (9) He, T.; Stolte, M.; Burschka, C.; Hansen, N. H.; Musiol, T.; Kälblein, D.; Pflaum, J.; Tao, X.; Brill, J.; Würthner, F. Single-crystal field-effect transistors of new Cl₂-NDI polymorph processed by sublimation in air. *Nat. Commun.* **2015**, *6*, 5954.
- (10) He, T.; Stolte, M.; Würthner, F. Air-Stable n-Channel Organic Single Crystal Field-Effect Transistors Based on Microribbons of Core-Chlorinated Naphthalene Diimide. *Adv. Mater.* **2013**, *25*, 6951–6955.
- (11) Oh, J. H.; Suraru, S.-L.; Lee, W. Y.; Kōnemann, M.; Höffken, H. W.; Röger, C.; Schmidt, R.; Chung, Y.; Chen, W.-C.; Würthner, F.; Bao, Z. High-performance air-stable n-type organic transistors based on core-chlorinated naphthalene tetracarboxylic diimides. *Adv. Funct. Mater.* **2010**, *20*, 2148–2156.
- (12) Davydov, A. S. THE THEORY OF MOLECULAR EXCITONS. *Sov. Phys. Uspekhi* **1964**, *7*, 145–178.
- (13) Laudise, R.; Kloc, C.; Simpkins, P.; Siegrist, T. Physical vapor growth of organic semiconductors. *J. Cryst. Growth* **1998**, *187*, 449–454.
- (14) Dressel, M.; Grüner, G. *Electrodynamics of Solids: Optical Properties of Electrons in Matter*; Cambridge University Press: Cambridge, U.K., 2002.
- (15) Tanner, D. B. *Optical Effects in Solids*; Cambridge University Press: Cambridge, U.K., 2019.
- (16) Wooten, F. *Optical properties of solids*; Academic Press: New York, 1972.
- (17) Roh, S.; Lee, S.; Lee, M.; Seo, Y.-S.; Khare, A.; Yoo, T.; Woo, S.; Choi, W. S.; Hwang, J.; Glamazda, A.; et al. Oxygen vacancy induced structural evolution of SrFeO_{3-x} epitaxial thin film from brownmillerite to perovskite. *Phys. Rev. B: Condens. Matter Mater. Phys.* **2018**, *97*, No. 075104.
- (18) Fleury, P. A. The Effects of Soft Modes on the Structure and Properties of Materials. *Annu. Rev. Mater. Sci.* **1976**, *6*, 157–180.
- (19) Lobo, R. P. S. M.; Moreira, R. L.; Lebeugle, D.; Colson, D. Infrared phonon dynamics of a multiferroic BiFeO₃ single crystal. *Phys. Rev. B: Condens. Matter Mater. Phys.* **2007**, *76*, 172105.
- (20) May, A. F.; Delaire, O.; Niedziela, J. L.; Lara-Curzio, E.; Susner, M. A.; Abernathy, D. L.; Kirkham, M.; McGuire, M. A. Structural phase transition and phonon instability in Cu₁₂Sb₄S₁₃. *Phys. Rev. B: Condens. Matter Mater. Phys.* **2016**, *93*, No. 064104.

- (21) Scheblykin, I. G.; Drobizhev, M. A.; Varnavsky, O. P.; Van Der Auweraer, M.; Vitukhnovsky, A. G. Reorientation of transition dipoles during exciton relaxation in J-aggregates probed by fluorescence anisotropy. *Chem. Phys. Lett.* **1996**, *261*, 181–190.
- (22) Mcrae, E. G.; Kasha, M. Enhancement of phosphorescence ability upon aggregation of dye molecules. *J. Chem. Phys.* **1958**, *28*, 721–722.
- (23) Basko, D. M.; Lobanov, A. N.; Pimenov, A. V.; Vitukhnovsky, A. G. Molecular arrangement of the Davydov-split dye aggregates. *Chem. Phys. Lett.* **2003**, *369*, 192–197.
- (24) Eisfeld, A.; Briggs, J. The J- and H-bands of organic dye aggregates. *Chem. Phys.* **2006**, *324*, 376–384.
- (25) Sumi, H. Exciton Polarons of Molecular Crystal Model. II. Optical Spectra. *J. Phys. Soc. Jpn.* **1975**, *38*, 825–835.
- (26) Spano, F. C.; Silvestri, L. Multiple mode exciton-vibrational coupling in H-aggregates: Synergistic enhancement of the quantum yield. *J. Chem. Phys.* **2010**, *132*, No. 094704.
- (27) Georgiev, S.; Mihailov, L.; Singh, J. Exciton self-trapping processes. *Pure Appl. Chem.* **1995**, *67*, 447–456.
- (28) Merdasa, A.; Jiménez, A. J.; Camacho, R.; Meyer, M.; Würthner, F.; Scheblykin, I. G. Single Lévy States-Disorder Induced Energy Funnels in Molecular Aggregates. *Nano Lett.* **2014**, *14*, 6774–6781.
- (29) Vlaming, S. M.; Malyshev, V. A.; Eisfeld, A.; Knoester, J. Subdiffusive exciton motion in systems with heavy-tailed disorder. *J. Chem. Phys.* **2013**, *138*, 214316.
- (30) Bloemsmas, E. A.; Vlaming, S. M.; Malyshev, V. A.; Knoester, J. Signature of Anomalous Exciton Localization in the Optical Response of Self-Assembled Organic Nanotubes. *Phys. Rev. Lett.* **2015**, *114*, 156804.
- (31) Feynman, R. P. Slow Electrons in a Polar Crystal. *Phys. Rev.* **1955**, *97*, 660–665.
- (32) Emin, D. Optical properties of large and small polarons and bipolarons. *Phys. Rev. B: Condens. Matter Mater. Phys.* **1993**, *48*, 13691–13702.
- (33) Srimath Kandada, A. R.; Silva, C. Exciton Polarons in Two-Dimensional Hybrid Metal-Halide Perovskites. *J. Phys. Chem. Lett.* **2020**, *11*, 3173–3184.
- (34) Ahmad, J.; Uwe, H. Small-polaron excitations in $\text{Ba}_{1-x}\text{K}_x\text{BiO}_3$ studied by optical reflectivity measurements. *Phys. Rev. B: Condens. Matter Mater. Phys.* **2005**, *72*, 125103.
- (35) Deskins, N. A.; Dupuis, M. Electron transport via polaron hopping in bulk TiO_2 : A density functional theory characterization. *Phys. Rev. B: Condens. Matter Mater. Phys.* **2007**, *75*, 195212.
- (36) van Mechelen, J. L. M.; van der Marel, D.; Grimaldi, C.; Kuzmenko, A. B.; Armitage, N. P.; Reyren, N.; Hagemann, H.; Mazin, I. I. Electron-Phonon Interaction and Charge Carrier Mass Enhancement in SrTiO_3 . *Phys. Rev. Lett.* **2008**, *100*, 226403.
- (37) Choi, W. S.; Yoo, H. K.; Ohta, H. Polaron Transport and Thermoelectric Behavior in La-Doped SrTiO_3 Thin Films with Elemental Vacancies. *Adv. Funct. Mater.* **2015**, *25*, 799–804.
- (38) Frodason, Y. K.; Johansen, K. M.; Vines, L.; Varley, J. B. Self-trapped hole and impurity-related broad luminescence in $\beta\text{-Ga}_2\text{O}_3$. *J. Appl. Phys.* **2020**, *127*, No. 075701.
- (39) He, T.; Wu, Y.; D'Avino, G.; Schmidt, E.; Stolte, M.; Cornil, J.; Beljonne, D.; Ruden, P. P.; Würthner, F.; Frisbie, C. D. Crystal step edges can trap electrons on the surfaces of n-type organic semiconductors. *Nat. Commun.* **2018**, *9*, 2141.
- (40) Genereux, F.; Leonard, S. W.; van Driel, H. M.; Birner, A.; Gösele, U. Large birefringence in two-dimensional silicon photonic crystals. *Phys. Rev. B: Condens. Matter Mater. Phys.* **2001**, *63*, 161101.
- (41) Bhupathi, P.; Hwang, J.; Martin, R. M.; Blankstein, J.; Jaworski, L.; Mulders, N.; Tanner, D. B.; Lee, Y. Aerogel waveplates. *Opt. Express* **2009**, *17*, 10599–10605.
- (42) Kuttner, P. Birefringence of Optical Materials in the Infrared Region. *Opt. Acta* **1981**, *28*, 1551–1558.
- (43) Kang, S.; Nakajima, S.; Arakawa, Y.; Konishi, G. I.; Watanabe, J. Large extraordinary refractive index in highly birefringent nematic liquid crystals of dinaphthyl-diacetylene-based materials. *J. Mater. Chem. C* **2013**, *1*, 4222–4226.
- (44) Lv, X.; Wang, P.; Yu, H.; Hu, Y.; Zhang, H.; Qiu, C.; Li, J.; Wang, X.; Liu, B.; Zhang, Y. Growth and optical properties of a promising Deep-ultraviolet birefringent crystal $\text{Ba}_2\text{Mg}(\text{BO}_3)_2$. *Opt. Mater. Express* **2019**, *9*, 3835–3842.
- (45) Reuter, M.; Vieweg, N.; Fischer, B. M.; Mikulicz, M.; Koch, M.; Garbat, K.; Dąbrowski, R. Highly birefringent, low-loss liquid crystals for terahertz applications. *APL Mater.* **2013**, *1*, No. 012107.
- (46) Evtushenko, Y. M.; Romashkin, S.; Trofimov, N.; Chekhlova, T. Optical Properties of TiO_2 Thin Films. *Phys. Procedia* **2015**, *73*, 100–107.
- (47) Arakawa, Y.; Nakajima, S.; Kang, S.; Shigeta, M.; Konishi, G.-i.; Watanabe, J. Design of an extremely high birefringence nematic liquid crystal based on a dinaphthyl-diacetylene mesogen. *J. Mater. Chem.* **2012**, *22*, 13908–13910.